

Chiral Transition Metal Clusters from Two Enantiomeric Schiff Base Ligands. Synthesis, Structures, CD spectra and Magnetic properties

Lin-Lin Fan,^a Fu-Sheng Guo,^a Lei Yun,^a Zhuo-Jia Lin,^a Radovan Herchel,^b Ji-Dong Leng,^a Yong-Cong Ou,^a and Ming-liang Tong^{*a}

^a*Key Laboratory of Bioinorganic and Synthetic Chemistry of Ministry of Education, State Key Laboratory of Optoelectronic Materials and Technologies, School of Chemistry and Chemical Engineering, Sun Yat-Sen University, Guangzhou 510275, China*

^b*Department of Inorganic Chemistry, Faculty of Science, Palacký University, tř. 17. listopadu 12, 771 46 Olomouc, Czech Republic*

Abstract: Two enantiomeric Schiff base ligands *R*-/*S*-H₂L *in situ* generated from the condensation of *o*-vanillin with *R*- or *S*-2-phenylglycinol were applied to assemble chiral multinuclear transition metal magnetic clusters for the first time. Four new enantiomerically pure chiral clusters, [NaMn₄(μ₃-O)(N₃)_{1.75}Br_{0.25}(*R*-L)₃(MeOH)₂(H₂O)₂][NaMn₄(μ₃-O)(N₃)₂(*R*-L)₃(MeOH)₂(H₂O)₂]Br₄ (**1R**), [NaMn₄(μ₃-O)(N₃)_{1.75}Br_{0.25}(*S*-L)₃(MeOH)₂(H₂O)₂][NaMn₄(μ₃-O)(N₃)₂(*S*-L)₃(MeOH)₂(H₂O)₂]Br₄ (**1S**), [Cu₆(*R*-L)₂(*R*-HL)₂(N₃)₅(MeOH)]NO₃·2MeOH·H₂O (**2R**) and [Cu₆(*S*-L)₂(*S*-HL)₂(N₃)₅(MeOH)]NO₃·2MeOH·H₂O (**2S**), have been synthesized and characterized by single crystal X-ray crystallography and CD spectroscopy.. Three Mn(III) in the Mn^{II}Mn^{III}₃ clusters of **1R** and **1S** are joined together through the μ₃-O bridge to form an oxo-centered Mn₃O unit. Three L²⁻ link four manganese atoms via the μ₂-*O,N,O*-bridging manner into a Mn^{II}Mn^{III}₃ cluster in a distorted tetrahedral geometry. Enantiomeric **2S** and **2R** are hexanuclear copper(II) clusters composed of a cubane-like Cu₄L₄ part with a dinuclear Cu₂(N₃)₂ unit capped on one of the faces of the Cu₄L₄ cubane via the μ_{1,1}-azide and phenolate bridges from the chiral ligands. Magnetic analysis reveals intracluster antiferromagnetic interaction between adjacent manganese ions in chiral oxo-centered Mn^{II}Mn^{III}₃ magnetic clusters for **1R** and **1S**, and dominating antiferromagnetic over weak ferromagnetic interactions in Cu₆ clusters in **2R** and **2S**.

Introduction

Chirality is of great significance in biology, chemistry and materials science. Chiral coordination compounds have attracted much attention owing to their specific physical/chemical properties in optical materials, enantioselective synthesis and asymmetric catalysis.¹ The observation of magneto-chiral dichroism (MChD) effect from chiral paramagnetic compounds² has urged materials scientists to prepare new multifunctional molecular materials of both chirality and magnetism coexisting within one molecule. Since the pioneering work on a family of single-molecule magnets (SMMs) with μ_3 -O-centered manganese clusters was reported by Christou, Brechin and co-workers,^{3,4a,c-g} there have been great interest in polynuclear oxo-centered metal complexes, especially in manganese clusters as SMMs in the last two decades.³⁻⁵ However only several oxo-centered manganese clusters crystallized in chiral space groups have been found,^{6a} yet fewer of them were revealed with naturally optical activity.^{6b} It is still a challenge to synthesize enantiopure transition metal clusters because of the difficulties in controlling chirality within the molecular structures and throughout the entire supramolecular networks.^{7,8}

We have successfully prepared a series of manganese clusters by the utilization of some achiral aminoalcohol ligands such as triethanolamine (teaH₃) and *N,N,N',N'*-tetrakis(2-hydroxyethyl) ethylenediamine (edteH₄), including an unprecedented giant heterometallic Cu₁₇Mn₂₈ cluster [Cu₁₇Mn₂₈O₄₀(tea)₁₂(HCO₂)₆(H₂O)₄].36H₂O with a $S = 51/2$ ground state in low magnetic field,^{9a} a novel family of Mn₁₂ clusters incorporating the same Mn₁₂O₄ cores and the tunable oxidation states of Mn^{III}_{*x*}Mn^{II}_{12-*x*} (*x* = 8, 10 and 12) with the increasing S_T values *versus* the increasing quantity of Mn^{III} ions,^{9b} and an unusual ferromagnetic tetranuclear Mn^{II}₂Mn^{IV}₂ compound with $S_T = 8$.^{9c} To further extend the studies on transition metal clusters, we now focus on the transition metal chemistry of chiral schiff base ligands. Schiff base metal complexes are a class of compounds that have been studied extensively due to their attractive physical/chemical properties and their wide-ranging applications.¹⁰ Salicylaldehyde derivated Schiff bases, which are potentially multi-dentate and hydroxyl-rich ligands, have not well been exploited for the preparation of polynuclear complexes.^{11,12} Herein we report the synthesis, structures and magnetic properties of two enantiomeric oxo-centered Mn^{II}Mn^{III}₃ compounds, [NaMn₄(μ_3 -O)(N₃)_{1.75}Br_{0.25}(*R*-

$\text{L})_3(\text{MeOH})_2(\text{H}_2\text{O})_2][\text{NaMn}_4(\mu_3\text{-O})(\text{N}_3)_2(\text{R-L})_3(\text{MeOH})_2(\text{H}_2\text{O})_2]\text{Br}_4$ (**1R**) and $[\text{NaMn}_4(\mu_3\text{-O})(\text{N}_3)_{1.75}\text{Br}_{0.25}(\text{S-L})_3(\text{MeOH})_2(\text{H}_2\text{O})_2][\text{NaMn}_4(\mu_3\text{-O})(\text{N}_3)_2(\text{S-L})_3(\text{MeOH})_2(\text{H}_2\text{O})_2]\text{Br}_4$ (**1S**), and two enantiomeric Cu^{II}_6 compounds, $[\text{Cu}_6(\text{R-L})_2(\text{R-HL})_2(\text{N}_3)_5(\text{MeOH})]\text{NO}_3 \cdot 2\text{MeOH} \cdot \text{H}_2\text{O}$ (**2R**) and $[\text{Cu}_6(\text{S-L})_2(\text{S-HL})_2(\text{N}_3)_5(\text{MeOH})]\text{NO}_3 \cdot 2\text{MeOH} \cdot \text{H}_2\text{O}$ (**2S**). The chiral ligands *R*-/*S*- H_2L (Scheme 1) in the four compounds were derived from the *in situ* condensation reaction of *o*-vanillin with (*R*)-(-)- or (*S*)-(+)-2-phenylglycinol, respectively.

Experimental Section

Materials and Physical Measurements The reagents and solvents used were commercially available and used as received without further purification. The Schiff-base ligands *R*- H_2L and *S*- H_2L were *in situ* generated from the condensation of *o*-vanillin with (*R*)-(-)-2-phenylglycinol or (*S*)-(+)-2-phenylglycinol, respectively. C, H, and N microanalyses were carried out with Elementar Vario-EL CHN elemental analyzer. FT-IR spectra were recorded in KBr tablets in the range of 4000–400 cm^{-1} on Bio-Rad FTS-7 spectrometer. Variable-temperature magnetic susceptibility measurements were carried out using SQUID magnetometer MPMS XL-7 (Quantum Design) at 0.1 T for **1R**, **1S**, **2R** and **2S**. Diamagnetic correction was applied from Pascal's constants. The circular dichroism spectra were recorded on a JASCO J-810 Spectropolarimeter in KBr pellets. The UV-vis spectra were measured on a JASCO V-570 spectrophotometer.

Caution Azido complexes are potentially explosive, especially in the presence of organic ligands. Therefore these compounds must be handled with care and prepared only in small amounts.

Synthesis of 1R or 1S. The mixture of *o*-vanillin (0.2 mmol), (*R*)-(-)-2-phenylglycinol (0.2 mmol)/(*S*)-(+)-2-phenylglycinol (0.2 mmol) and NaN_3 (0.8 mmol, 0.052 g) was added to the methanolic solution (10 mL) of $\text{MnBr}_2 \cdot 4\text{H}_2\text{O}$ (0.8 mmol, 0.229 g) at room temperature. A clear solution in brown color was yielded after stirring for 2 hours. The resulted solution was allowed to evaporate slowly in air. Well-shaped black crystals of **1R** or **1S** were collected in one week. Yield: 61 mg (63%) for **1R** and 63 mg (65%) for **1S**. Elemental analysis calcd (%) for $\text{C}_{102}\text{H}_{122}\text{Br}_{4.25}\text{Mn}_8\text{N}_{17.25}\text{Na}_2\text{O}_{30}$ (**1R**): C, 42.32; H, 4.25; N, 8.35; found (%): C, 41.92; H, 4.39; N, 8.73%. IR (KBr cm^{-1}): 3408 (br), 2051 (s), 1618 (s), 1384 (s), 1020 (m), 642 (w).

Elemental analysis calcd (%) for $C_{102}H_{122}Br_{4.25}Mn_8N_{17.25}Na_2O_{30}$ (**1S**): C, 42.32; H, 4.25; N, 8.35; found (%): C, 42.18, H 4.31, N 8.80%.

Synthesis of 2R or 2S. The mixture of *o*-vanillin (0.2 mmol), (*R*)-(-)-2-phenylglycinol (0.2 mmol)/(*S*)-(+)-2-phenylglycinol (0.2 mmol) and NaN_3 (0.5 mmol, 0.039 g) was added to the methanolic solution (10 mL) of $Mn(NO_3)_2 \cdot 4H_2O$ (0.3 mmol, 0.075 g) and $Cu(NO_3)_2 \cdot 3H_2O$ (0.2 mmol, 0.048 g) at room temperature. A dark-green solution was observed after stirring for 2 hours and allowed to evaporate slowly in air. Well-shaped dark green crystals of **2R** or **2S** were collected in three days. Yield: 19 mg (31%) for **2R** and 21 mg (34%) for **2S**. Elemental analysis calcd (%) for $C_{67}H_{76}Cu_6N_{20}O_{19}$ (**2R**): C, 43.58; H, 4.15; N, 15.17; found (%): C, 43.09; H, 3.95; N, 15.46%. IR (KBr cm^{-1}): 3423 (br), 2075 (s), 1637 (s), 1384 (m), 1171 (s), 742 (m). Elemental analysis calcd (%) for $C_{67}H_{76}Cu_6N_{20}O_{19}$ (**2S**): C, 43.58; H, 4.15; N, 15.17; found (%): C, 43.41, H, 4.00, N, 15.41%.

X-ray Crystallography Diffraction data were recorded on Oxford Diffraction Gemini R CCD diffractometer with Cu $K\alpha$ radiation ($\lambda = 1.54178 \text{ \AA}$) for **1R**, **1S** and **2S** and on Bruker Apex CCD area detector diffractometer with Mo $K\alpha$ radiation ($\lambda = 0.71073 \text{ \AA}$) for **2R** at 150 K. The temperature of measurement was controlled using Oxford Cryosystems Cryostream cooling apparatus. The data procession was accomplished with the program SAINT; absorption correction based on symmetry equivalent reflections was applied using the SADABS program for **2R**.^{13a} The data collection routine, unit cell refinement, and data processing were carried out with the program CrysAlisPro for **1S**, **1R** and **2S**.^{13b} The structures were solved by direct method and all non-hydrogen atoms were refined anisotropically by full-matrix least-squares techniques using the SHELXTL program.¹⁴ The hydrogen atoms on the organic motifs were added on calculated positions and refined with isotropic thermal parameters riding on those of the parent atoms. These idealized H atoms had their isotropic temperature factors fixed at 1.2 or 1.5 times the equivalent isotropic U of the parent C atoms to which they were bonded. Further details for structural analysis for compounds **1R**, **1S**, **2S** and **2R** are summarized in Table 1. Bond distances and angles are listed in Tables S1 and S2 in the Supporting Information.

CCDC reference numbers 721497 & 721498 and 750370 & 750371.

For crystallographic data in CIF or other electronic format see DOI: 10.1039/B917091J

Results and Discussion

Synthesis.

Both **1R** and **1S** contain the Mn^{III} ions. Given that the starting Mn sources were exclusively Mn^{II} ions, it is apparent that the Mn^{III} ions were generated upon the oxidation by atmospheric O₂, a process very common in manganese cluster chemistry even in solvents with moderate reducibility.¹² There are N₃⁻/Br⁻ disorder observed in the structures, but we have tried in vain to replace Br⁻ ion and avoid the disorder by increasing the amount of N₃⁻ to 1.0 mmol or starting from manganese salts with weakly-coordinated anions such as Mn(NO₃)₂·6H₂O and Mn(ClO₄)₂·6H₂O. The combination of MnBr₂·4H₂O/NaN₃ as the metal sources and Lewis bases seemingly works the best to yield the clusters. When Mn(OAc)₂·4H₂O/NaOAc·3H₂O were used in the reaction where the acetate was expected to take the place of the bridging N₃⁻/Br⁻, or when MnBr₂·4H₂O/Et₃N were involved where the manganese cations, Mn(III) or Mn(II), was supposed to replace the sodium ion, only amorphous powder were yielded.

It should be noted that Mn(II) salt is the necessary for the synthesis of compounds **2R** and **2S** though the component of final products do not contain any Mn element. Only amorphous power precipitate was obtained in the absence of manganese(II) salts.

Crystal structures

Structures of 1R and 1S. X-ray single crystal structure analysis reveals that **1R** and **1S** are enantiomeric to each other and crystallize in monoclinic space group *P2*₁. There are two cationic Mn₄ cluster units and four Br⁻ anions within an asymmetric unit (Figure 1a) in **1R/1S**. The two manganese clusters are almost the same except that in the first cluster one azide in an end-on mode is connected between two Mn^{III} atoms while in the second manganese cluster, there is some disorder on the bridge ligands between two Mn^{III} ions with 75% end-on azide and 25% μ₂-bromide ions occupancy. Each manganese cluster is composed of four crystallographically unique Mn atoms, three Mn^{III} and one Mn^{II}. In one of the clusters, the Mn^{III} atoms, Mn1, Mn2 and Mn3, are joined together through the μ₃-O bridge to form an oxo-centered Mn₃O unit. Mn1

and Mn3 have almost the same coordination environments in slightly distorted octahedral geometry surrounded with one $R-L^{2-}$ via O,N,O -chelation, one μ_3 -O atom, one μ_2 -MeOH and one N_3^-/Br^- ion (Mn1-O = 1.850(9)-2.505(11) Å, Mn1-N(Br) = 1.967(13)-2.828(7) Å, Mn3-O = 1.884(11)-2.592(11) Å, Mn3-N(Br) = 2.001(13)-2.661(7) Å). Mn2 is adapted in an octahedral geometry coordinated with one μ_3 -O, two μ_2 -MeOH and one O,N,O -dentate $R-L$ (Mn2-O = 1.847(9)-2.473(12) Å, Mn2-N = 1.956(11) Å). Two μ_2 -MeOHs and one μ_2 - N_3^- bridging help the Mn_3O core to retain the trigonal geometry. The only Mn^{II} atom, Mn4, shows a slightly distorted octahedral geometry connected by three μ_2 -O atoms from three $R-L^{2-}$ ligands (Mn4-O = 2.168(11)-2.201(10) Å), two water molecules (Mn4-O = 2.256(12)-2.260(13) Å) and one N_3^- (Mn4-N = 2.178(15) Å). The chirality of the organic ligands was retained during the reactions and the six L s in the asymmetric unit are in the same handedness. Three $R-L^{2-}$ link four manganese atoms via the μ_2 - O,N,O -bridging manner into a $Mn^{II}Mn^{III}_3$ cluster in a distorted tetrahedral geometry (Figure 1b). The sodium atom is encapsulated by the deprotonated hydroxyl groups and the methoxyl groups on the tails of three R - L s beneath the tetrahedral $Mn^{II}Mn^{III}_3$ core and thus forms a trigonal bipyramidal $Mn^{II}Mn^{III}_3Na$ cluster.

Structures of 2R and 2S

Enantiomeric compounds **2R** and **2S** crystallize in orthorhombic space group $P2_12_12_1$. The asymmetric unit contains one discrete hexanuclear Cu_6 cluster cation, one NO_3^- counterion, one lattice water and two solvated methanol molecules (Figure 2). The cationic Cu_6 core is composed of six crystallographically unique Cu atoms on general positions, two completely deprotonated L^{2-} and two mono-deprotonated HL^- ligands, three end-on and two terminal N_3^- and one coordinated methanol molecule. The Cu1, Cu4 and Cu5 have the similar elongated [4+1] square pyramidal geometry. Cu1 is surrounded with one mono-deprotonated HL^- via the O,N,O -chelation, one L^{2-} via the deprotonated μ_3 -hydroxide and one methanol molecule (Cu1- O_{R-L} = 1.930(6)-1.990(6) Å, Cu1- O_{MeOH} = 2.233(7) Å, Cu1- N_{R-L} = 1.940(7) Å for **2R**; Cu1- O_{S-L} = 1.938(4)-1.991(4) Å, Cu1- O_{MeOH} = 2.243(4) Å, Cu1- N_{S-L} = 1.943(5) Å for **2S**). Cu4 has the similar coordination environment except that the methanol is replaced with the end-on azide (Cu4-O = 1.948(6)-1.975(6) Å, Cu4- N_{R-L} = 1.933(7) Å and Cu4- N_{azide} = 2.299(8) Å for **2R**; Cu4-O = 1.935(4)-1.987(4) Å, Cu4- N_{S-L} = 1.949(5) Å and Cu4- N_{azide} = 2.306(5) Å for **2S**). Cu5 is connected with one deprotonated L^{2-} via the

O,O-chelation and three end-on azides (Cu5-O_{R-L} = 2.009(6) and 2.288(7) Å, Cu5-N_{azide} = 1.946(8)-2.000(8) Å for **2R**; Cu5-O_{S-L} = 2.024(4) and 2.275(5) Å, Cu5-N_{azide} = 1.958(6)-2.005(6) Å for **2S**). The Cu2 and Cu3 atoms are in a similar elongated [4+2] octahedral geometry linked with one HL⁻ via *O,O*-chelation and two L²⁻ via the *O,N,O*-chelation and the μ₃-hydroxide (Cu2-O_{R-L} = 1.886(6)-2.548(6) Å, Cu2-N_{R-L} = 1.941(7) Å; Cu3-O_{R-L} = 1.936(6)-2.466(6) Å, Cu3-N_{R-L} = 1.925(7) Å for **2R**; Cu2-O_{S-L} = 1.903(4)-2.545(4) Å, Cu2-N_{S-L} = 1.914(7) Å; Cu3-O_{S-L} = 1.947(4)-2.470(4) Å, Cu3-N_{S-L} = 1.921(5) Å for **2S**). Cu6 has a square planar geometry coordinated with two end-on and two terminal azide ligands (Cu6-N_{azide} = 1.943(9)-1.998(8) Å for **2R**; Cu6-N_{azide} = 1.958(7)-2.019(6) Å for **2S**). The Cu5 and Cu6 are bridged by two μ_{1,1}-azides into a dinuclear Cu₂(N₃)₂ with the Cu⋯Cu distances of 3.092(2) for **2R** and 3.102(1) Å for **2S**, respectively. Both HL⁻ ligands link two copper centers in *O(H),N,O*- and *O,O*-chelation fashion while one of the L²⁻ ligands connects three metal ions in *O,N,O*-chelation and μ₃-O modes and the other links four copper in a μ₃-O, μ₃-*O,N*, μ₂-*O*- and μ₂-*O,O*-chelation manner. Accordingly the Cu₆ cluster can be viewed as constructing from two units: a cubane-like Cu₄O₄-containing part with a dinuclear Cu₂(N₃)₂ unit capped on one of the faces of the Cu₄O₄ cubane via the μ_{1,1}-azide and phenolate bridges. The Cu⋯Cu distances within the Cu₄O₄ unit are 3.150(2)-3.897(2) for **2R** and 3.167(1)-3.900(1) Å for **2S**, respectively. The dihedral angle between the dinuclear Cu₂(N₃)₂ motif and the capped face of Cu₄O₄ cubane unit is ca. 5.489°. No symmetric relationship can be found between the copper atoms in either the Cu₄O₄ cubane or Cu₆ cluster. This is quite different from the previously reported double-capped cubane Cu₆ compound,¹⁵ in which both the cubane and the Cu₆ cluster have the S₄ symmetry.

Spectroscopic Properties

Enantiopurity of the chiral organic ligands and the resulted coordination compounds was investigated with circular dichroism (CD) spectroscopy. The starting materials, (*R*)-(-)/(*S*)-(+)-2-phenylglycinol, exhibit absorption peaks at 260 nm and 270 nm in methanol solution, which are due to π-π* transitions of benzene rings (Figure S1a). The CD spectra of Schiff base *R*-H₂L/*S*-H₂L (the mixture of *o*-vanillin and (*R*)-(-)/(*S*)-(+)-2-phenylglycinol in molar ratio of 1:1 in methanol) are rather different from those for 2-phenylglycinol, which have the contiguous peaks of the same sign at wavelength of 325 nm and 418 nm (Figure S1b). These

absorption are attributed to $\pi-\pi^*$ transitions and $n-\pi^*$ transitions originating from the azomethine chromophore of Schiff base *R*-H₂L/*S*-H₂L.

The enantiomeric nature of **1R** and **1S** in solid state was measured using circular dichroism spectroscopy in KBr pellets (Figure 3a). The spectra of **1R** and **1S** are mirror-image to each other. The *R*-enantiomer exhibits a small positive absorption at 260nm, decreases to a large negative peak at 320 nm and increases again to a positive maximum at 425nm. The *S*-enantiomer displays absorption peaks of the opposite sign in the same wavelength range. The CD spectra of **1R** and **1S** in methanol solution were also studied, which are similar in shape to those measured in solid state except that the absorption maxima shift to 300 nm and 400 nm for **1R** and **1S** (Figure S1c). The three peaks of **1R** and **1S** both in solid and solution states are attributed to $\pi-\pi^*$ transitions of benzene ring, $\pi-\pi^*$ transitions and $n-\pi^*$ transitions originating from the azomethine chromophore from higher energy region to the lower one.

The circular dichroism (CD) spectra of **2R** and **2S** were measured in KBr pellets as well as in methanol solution (Figure 3b and S1d). The solid state CD spectrum of **2R** exhibits three weak positive absorption peaks at 265 nm, 400 nm and 600 nm and two negative dichroic signals centered at 300 nm and 465 nm. **2S** shows Cotton effects of the opposite sign at the same wavelengths. The CD spectra of **2R** and **2S** in methanol are similar to those in KBr pellets except that the peaks at 265 nm are absent. The bands near 300 nm, 400 nm, 450 nm and 600 nm generally correspond to $\pi-\pi^*$ transitions of benzene ring, $\pi-\pi^*$ transitions and $n-\pi^*$ transitions originating from the azomethine chromophore and d-d transitions, respectively.¹⁶

The UV spectrum of **1S** recorded in methanol solution shows three bands at 275 nm, 310 nm with shoulders on their low-energy sides and a broad peak near 400 nm, which are in accordance with the CD spectra. The UV spectrum of **2R** exhibits three bands near 280 nm, 380 nm and 680 nm (Figure S2).

Magnetic Properties

The magnetic properties of compounds **1R**, **1S**, **2R** and **2S** were investigated between 2K and 300 K using Quantum Design SQUID magnetometer MPMS XL-7. Both enantiomorphous **1R** and **1S** have similar magnetic behaviors, suggesting that the chirality of **1R** and **1S** have very little influence on the magnetism of them (Figure 4a,b). There exhibits a decrease of the magnetic moment value as the temperature drops,

indicating the presence of dominant antiferromagnetic interaction between the manganese spins (Figure 4c). Because the two $\text{Mn}^{\text{II}}\text{Mn}^{\text{III}}_3$ clusters in the asymmetric unit have only small difference in the terminal ligands (the N_3^- and disordered N_3^-/Br), they were treated using the same Mn_4 model (Scheme 2a). The four units are one $\{\text{Mn}^{\text{II}}\text{O}_5\text{N}\}$, one $\{\text{Mn}^{\text{III}}\text{O}_5\text{N}\}$ and two $\{\text{Mn}^{\text{III}}\text{O}_4\text{NBr}\}$ respectively, corresponding to $S_4 = 5/2$ (Mn^{II}), $S_1 = S_2 = S_3 = 2$ (Mn^{III}). The susceptibility was simulated on the basis of their molecular structures in the frame of an isotropic Heisenberg model, similar to that used in the analogous Mn_4 clusters reported by Powell *et al.*¹² As for the six non-equivalent couplings, similar bridges between the manganese ions were considered to be identical in the fitting and bridging modes. The best-fit parameters obtained within the isotropic model are $J_1 = -2.9 \text{ cm}^{-1}$, $J_2 = -14.0 \text{ cm}^{-1}$, $J_3 = -12.0 \text{ cm}^{-1}$, $g_{\text{Mn(II)}} = g_{\text{Mn(III)}} = 2.0$ (fixed). The crucial factor for improving the overall fit is inclusive of the zero-field terms for Mn(III) centers using the modified Spin Hamiltonian as $\hat{H}_a = -J_1(S_1 \cdot S_4 + S_2 \cdot S_4 + S_3 \cdot S_4) - J_2(S_1 \cdot S_2 + S_2 \cdot S_3) - J_3(S_1 \cdot S_3) + \sum S_i \cdot D_i \cdot S_i + \mu_B \sum S_i \cdot B_a \cdot g_i$. The best-fit parameters are $J_1 = -3.3 \text{ cm}^{-1}$, $J_2 = -12.7 \text{ cm}^{-1}$, $J_3 = -14.8 \text{ cm}^{-1}$, $g_{\text{Mn(II)}} = g_{\text{Mn(III)}} = 2.0$ (fixed) and $D_{1,\text{Mn(III)}} = D_{2,\text{Mn(III)}} = D_{3,\text{Mn(III)}} = +5.0 \text{ cm}^{-1}$ (Figure 4c). It should be noted that the J values obtained from both computing models are comparable though the fitting results are not perfectly well due to the presence of two sets of $\text{Mn}^{\text{II}}\text{Mn}^{\text{III}}_3$ units within the asymmetric unit. The small difference in the bond angles and distances among manganese centers have been ignored and simplified to one set of parameters. All the J values are negative in both simulated models, suggesting that anti-ferromagnetic coupling occurs between the adjacent Mn centers and both compounds **1R** and **1S** possess $S_T = 1/2$ ground state. Though there is an azide bridging in the end-on fashion between Mn1 and Mn3, it is too weak to influence the interactions compared with the μ_3 -O bridge. The D parameter in the best fit is positive and the attempts to fit the susceptibility data with negatives values of D failed.

The members of triangular $[\text{Mn}^{\text{III}}_3\text{O}(\text{O}_2\text{CR})_6\text{L}_3]^+$ complexes containing the $[\text{Mn}_3(\mu_3\text{-O})]$ core are non-negligible as a part of SMMs family.⁴ Milios, Brechin and co-workers discovered for the manganese salicylaldoxime complexes that the Mn–N–O–Mn torsion angles (α) on the $[\text{Mn}_3(\mu_3\text{-O})]$ trinuclear moieties are highly correlative to the ground-state spin values of the complexes and accordingly, the sign of the magnetic interaction between neighboring Mn atoms.^{4a,f} Nevertheless, no such torsion angles can be found

in Schiff base complexes **1R** and **1S**. Another distinct difference between the SMMs with $[\text{Mn}_3(\mu_3\text{-O})]$ cored and **1R/1S** is the orientation of the Jahn–Teller axes of the manganese atoms. The axes on the SMMs are approximately parallel to each other and arrayed perpendicular to the $[\text{Mn}_3(\mu_3\text{-O})]$ planes while in **1R/1S**, the Jahn–Teller axes are aligned on the $[\text{Mn}_3(\mu_3\text{-O})]$ planes. $D > 0$ is in agreement with the absence of SMM properties.

Both enantiomorphous **2R** and **2S** have very similar magnetic behaviors, suggesting that the chirality has almost no influence on the magnetism of **2R** and **2S** (Figure 5a,b). The value of μ_{eff} is $4.3 \mu_{\text{B}}$ per Cu_6 unit for **2R** at room temperature, which is in agreement with the expected sum of six non-interacting Cu^{2+} ($S = 1/2$) cations ($4.2 \mu_{\text{B}}$ for $g = 2.0$). Upon cooling the sample, the μ_{eff} decreases to a minimum value at 20 K and gradually turns up, indicative of the presence of dominant antiferromagnetic and weak ferromagnetic interactions between the copper spins within Cu_6 core. In order to reduce the number of parameters and avoid overparameterization,^{15,17} we supposed that two exchange parameters J_1 (via three short Cu-O bonds) and J_2 (via two short Cu-O bonds) are associated with the intracubane Cu-O-Cu exchanges, another two exchange parameters (J_3 and J_4) are associated with the cubane- $\text{Cu}_2(\text{N}_3)_2$ Cu-O-Cu and Cu- N_{azide} -Cu exchanges, respectively, and the fifth exchange parameter (J_5) is associated with the intra- $\text{Cu}_2(\text{N}_3)_2$ Cu- N_{azide} -Cu exchange (Scheme 2b). A full analysis of the magnetic exchange interactions has been performed using the full-matrix diagonalization program MAGPACK¹⁸ with the Hamiltonian $\hat{H} = -2J_1(\mathbf{S}_1 \cdot \mathbf{S}_2 + \mathbf{S}_2 \cdot \mathbf{S}_4 + \mathbf{S}_1 \cdot \mathbf{S}_3 + \mathbf{S}_3 \cdot \mathbf{S}_4) - 2J_2\mathbf{S}_2 \cdot \mathbf{S}_3 - 2J_3\mathbf{S}_3 \cdot \mathbf{S}_5 - 2J_4\mathbf{S}_4 \cdot \mathbf{S}_5 - 2J_5\mathbf{S}_5 \cdot \mathbf{S}_6$. The best-fitted values are $g = 2.12$, $J_1 = -75.0 \text{ cm}^{-1}$, $J_2 = +1.8 \text{ cm}^{-1}$, $J_3 = -67.8 \text{ cm}^{-1}$, $J_4 = 5.8 \text{ cm}^{-1}$ and $J_5 = 8.2 \text{ cm}^{-1}$ (Figure 5c). This analysis leads to the conclusion that both compounds **2R** and **2S** possess $S_T = 1$ ground state, which is in the agreement with the isothermal magnetization saturation value (Figure 5b).

The irregular cubane Cu_4O_4 cores within compounds **2R** and **2S** are characteristic of five short (3.1886(15)- 3.3274(14) Å for **2R** and 3.1667(12)-3.3859(11) Å for **2S**) and one long Cu \cdots Cu distances (3.897 Å for **2R** and 3.9002 Å for **2S**), which is different from those reported types of cubane structures such as the 2 + 4 class, 4 + 2 class and 6 + 0 class based on the length of the Cu \cdots Cu separation as a classification criterion proposed by Javier Tercero *et al.*¹⁹ From a $[\text{Cu}_4(\mu\text{-OMe})_4(\text{NH}_3)_8]^{4+}$ model

corresponding to those 4+2 cubane compounds, the calculated J coupling constant corresponding to the exchange pathway with two short Cu-O bond distances may result in either ferromagnetic or antiferromagnetic interactions depending on the value of the Cu-O-Cu angle (β). An increase in the Cu-O-Cu angle finally leads to antiferromagnetic coupling for $\beta \approx 104^\circ$. For **2R**, as the β is significantly larger than 104° , antiferromagnetic interaction is predicted.²⁰ Compared with the result of Jäger and Klemm ($\beta = 99.3\text{-}102.9^\circ$, $J = -50 \text{ cm}^{-1}$),²¹ which is in agreement with the above experimental data fitting results of $J_1 = -75.0 \text{ cm}^{-1}$. The Cu3-O-Cu5 exchange pathway also transmits a moderate antiferromagnetic interaction with the exchange parameter of $J_3 = -67.8 \text{ cm}^{-1}$. The exchange parameter of $J_4 = 5.8 \text{ cm}^{-1}$ for the asymmetric Cu4-N_{azide}-Cu5 exchange pathway corresponds to weak ferromagnetic coupling due to the perpendicular orientation of the magnetic orbital. The symmetric Cu5-($\mu_{1,1}$ -azido)₂-Cu6 exchange pathway with the Cu-N_{azido}-Cu angles (θ) of $101.4(4)^\circ$ and $103.2(4)^\circ$, which are less than 108.8° , is predicted to be ferromagnetic.^{22a} Eliseo Ruiz and coworkers discussed the relation between the J values and the Cu-N-Cu angle (θ) as well as the out-of-plane deviation of the azido group (τ) for the azido-bridged compounds. One double end-on azido-bridged complex with $\theta = 104.6^\circ$, $\tau = 16.6^\circ$ and calculated $J = +5 \text{ cm}^{-1}$ has been reported,^{22b} which is similar to **2R** with $\theta = 101.4^\circ/103.2(4)^\circ$, $\tau = 10.6^\circ/17.9^\circ$ and $J_5 = +8.2 \text{ cm}^{-1}$.

Conclusion

We have prepared and characterized four enantiomerically pure chiral polynuclear transition metal complexes with Schiff base ligands *R*- and *S*-H₂L. **1R** and **1S** are tetranuclear clusters with three Mn(III) ions and one Mn(II) ion combined via μ_3 -O and *R*-/*S*-H₂L ligands. Enantiomeric **2S** and **2R** are capped-cubane Cu₆O₅N₃ clusters with the phenoxo group and N₃⁻ as bridges to link the “cubane” and “cap”. The enantiomeric nature of **1R**, **1S**, **2R** and **2S** was confirmed via CD spectroscopy. Magnetic investigation reveals that antiferromagnetic interactions occur between adjacent manganese ions in **1R** and **1S**. An overall antiferromagnetic coupling was found for **2R** and **2S** via competition of the slightly dominating intra-cubane antiferromagnetic interaction and the cubane-Cu₂(N₃)₂ antiferromagnetic exchange over the intra-Cu₂(N₃)₂

ferromagnetic interaction through the double $\mu_{1,1}$ -N₃ bridges. Our results suggest a promising strategy to synthesize molecular magnets with chirality towards the MChD effect.

Acknowledgment. This work was supported by the NSFC (grant nos 20525102, 20821001, 50872157, 90922009 and J0730420), the “973 Project” (2007CB815305), and the Czech Ministry of Education, Youth and Sports (Grant No. MSM6198959218).

References

- 1 (a) U. Knof and A. von Zelewsky, *Angew. Chem., Int. Ed.*, 1999, **38**, 302; (b) G. Desimoni, G. Faita and P. Quadrelli, *Chem. Rev.*, 2003, **103**, 3119; (c) J. Chin, S. S. Lee, K. J. Lee, S. Park and D. H. Kim, *Nature*, 1999, **401**, 254; (d) H.-R. Wen, C.-F. Wang, Y. Song, J.-L. Zuo and X.-Z. You, *Inorg. Chem.*, 2005, **44**, 9039; (e) L. D. Barron, *Nature*, 2000, **405**, 895; (f) G. L. J. A. Rikken and E. Raupach, *Nature*, 2000, **405**, 932. (g) B. Zhang, Z. Wang, M. Kurmoo, S. Gao, K. Inoue and H. Kobayashi, *Adv. Funct. Mater.*, 2007, **17**, 577.
- 2 (a) G. L. J. A. Rikken and E. Raupach, *Nature*, 1997, **390**, 493. (b) C. Train, R. Gheorghe, V. Krstic, L.-M. Chamoreau, N. S. Ovanesyan, G. L. J. A. Rikken, M. Gruselle and M. Verdaguer, *Nature Mater.*, 2008, **7**, 729.
- 3 N. A. Alcalde, R. S. Edwards, S. O. Hill, W. Wernsdorfer, K. Folting and G. Christou, *J. Am. Chem. Soc.*, 2004, **126**, 12503.
- 4 (a) R. Inglis, L. F. Jones, C. J. Milios, S. Datta, A. Collins, S. Parsons, W. Wernsdorfer, S. Hill, S. P. Perlepes, S. Piligkos and E. K. Brechin, *Dalton. Trans.* 2009, **18**, 3403; (b) C. J. Milios, C. P. Raptopoulou, A. Terzis, F. Lloret, R. Vicente, S. P. Perlepes, and A. Escuer, *Angew. Chem. Int. Ed.* 2004, **43**, 210; (c) C. J. Milios, R. Inglis, L. F. Jones, A. Prescimone, S. Parsons, W. Wernsdorfer and E. K. Brechin, *Dalton Trans.*, 2009, 2812; (d) S. G. Sreerama and S. Pal, *Inorg. Chem.* 2002, **41**, 4843; (e) T. C. Stamatatos, D. F. Albiol, C. C. Stoumpos, C. P. Raptopoulou, A. Terzis, W. Wernsdorfer, S. P. Perlepes and G. Christou, *J. Am. Chem. Soc.* 2005, **127**, 15380; (f) C. J. Milios, A. Vinslava, P. A. Wood, S. Parsons, W. Wernsdorfer, G. Christou, S. P. Perlepes and E. K. Brechin,

- J. Am. Chem. Soc.* 2007, **129**, 8; (g) C. J. Milios, R. Inglis, L. F. Jones, A. Prescimone, S. Parsons, W. Wernsdorfer and E. K. Brechin, *Dalton Trans.*, 2009, 2812.
- 5 (a) D. Gatteschi and R. Sessoli, *Angew. Chem. Int. Ed.*, 2003, **42**, 268; (b) T. Lis, *Acta Cryst.* 1980, **B36**, 2042; (c) A. Caneschi, D. Gatteschi, R. Sessoli, A.-L. Barra, L.-C. Brunel and M. Guillot, *J. Am. Chem. Soc.*, 1991, **113**, 5873; (d) R. Sessoli, D. Gatteschi, A. Caneschi and M. A. Novak, *Nature* 1993, **365**, 141; (e) R. Sessoli, H.-L. Tsai, A. R. Shake, S. Wang, J. B. Vincent, K. Folting, D. Gatteschi, G. Christou and D. N. Hendrickson, *J. Am. Chem. Soc.* 1993, **115**, 1804; (f) G. Rogez, B. Donnio, E. Terazzi, J.-L. Gallani, J.-P. Kappler, J.-P. Bucher and M. Drillon, *Adv. Mater.* 2009, **21**, advance articles; (g) K. Awaga, Y. Suzuki, H. Hachisuka and K. Takeda, *J. Mater. Chem.*, 2006, **16**, 2516; (h) H. Miyasaka, N. Matsumoto, H. Ōkawa, N. Re, E. Gallo, C. Floriani, *J. Am. Chem. Soc.* 1996, **118**, 981; (i) B. J. Kennedy; K. S. Murray, *Inorg. Chem.*, 1985, **24**, 1552; (j) B. J. Kennedy; K. S. Murray, *Inorg. Chem.*, 1985, **24**, 1557; (k) K. Bertocello, G. D. Fallon, K. S. Murray, E. R. T. Tiekink, *Inorg. Chem.*, 1991, **30**, 3562.
- 6 (a) K. C. Mondal, M. G. B. Drew and P. S. Mukherjee, *Inorg. Chem.*, 2007, **46**, 5625; (b) P. Gerbier, N. Domingo, J. Gómez-Segura, D. Ruiz-Molina, D. B. Amabilino, J. Tejada, B. E. Williamson and J. Veciana, *J. Mater. Chem.*, 2004, **14**, 2455.
- 7 (a) W. Kaneko, S. Kitagawa and M. Ohba, *J. Am. Chem. Soc.* 2007, **129**, 248; (b) H.-R. Wen, C.-F. Wang, Y.-Z. Li, J.-L. Zuo, Y. Song and X.-Z. You, *Inorg. Chem.*, 2006, **45**, 7032; (c) E.-Q. Gao, Y.-F. Yue, S.-Q. Bai, Z. He and C.-H. Yan, *J. Am. Chem. Soc.*, 2004, **126**, 1419; (d) H. Imai, K. Inoue, K. Kikuchi, Y. Yoshida, M. Ito, T. Sunahara and S. Onaka, *Angew. Chem., Int. Ed.*, 2004, **43**, 5618; (e) K. Inoue, K. Kikuchi, M. Ohba and H. Ōkawa, *Angew. Chem., Int. Ed.*, 2003, **42**, 4810; (f) M. Minguet, D. Luneau, E. Lhotel, V. Villar, C. Paulsen, D. B. Amabilino and J. Veciana, *Angew. Chem., Int. Ed.*, 2002, **41**, 586; (g) E. Coronado, C. J. Gómez-García, A. Nuez, F. M. Romero and J. C. Waerenborgh, *Chem. Mater.*, 2006, **18**, 2670; (h) M. Akita-Tanaka, H. Knmagai, A. Markosyan and K. Inoue, *Bull. Chem. Soc. Jpn.*, 2007, **80**, 204; (i) Y. Numata and K. Inoue, *Chem. Lett.*, 2007, **36**, 534; (j) M. Gruselle, C. Train, K. Boubekeur, P. Gredin and N. Ovanesyan, *Coord. Chem. Rev.*,

- 2006, **250**, 2491; (k) D. Armentano, G. De Munno, F. Lloret, A. V. Pali and M. Julve, *Inorg. Chem.*, 2002, **41**, 2007.
- 8 (a) Z.-G. Gu, Y. Song, J.-L. Zuo, X.-Z. You, *Inorg. Chem.* 2007, **46**, 9522; (b) M. Kato, A. K. Sah, T. Tanase, M. Mikuriya, *Inorg. Chem.* 2006, **45**, 6646; (c) Z.-M. Zhang, Y.-G. Li, S. Yao, E.-B. Wang, Y.-H. Wang, R. Clérac, *Angew. Chem. Int. Ed.* 2009, **48**, 1581; (d) N. Hoshino, T. Shiga, M. Nihei, H. Oshio, *Polyhedron*, 2009, **28**, 1754.
- 9 (a) W.-G. Wang, A.-J. Zhou, W.-X. Zhang, M.-L. Tong, X.-M. Chen, M. Nakano, C. C. Beedle and D. N. Hendrickson, *J. Am. Chem. Soc.*, 2007, **129**, 1014; (b) A.-J. Zhou, L.-J. Qin, C. C. Beedle, S. Ding, M. Nakano, J.-D. Leng, M.-L. Tong and D. N. Hendrickson, *Inorg. Chem.*, 2007, **46**, 8111; (c) A.-J. Zhou, J.-L. Liu, R. Herchel, J.-D. Leng and M.-L. Tong, *Dalton Trans.*, 2009, 3182.
- 10 (a) R. Noyori, *Science*, 1990, **248**, 1194; (b) Y. N. Belokon, S. C.-Cepas, B. Green, N. S. Ikonnikov, V. N. Khrustalev, V. S. Larichev, M. A. Moscalenko, M. North, C. Orizu, V. I. Tararov, M. Tasinazzo, G. I. Timofeeva and L. V. Yashkina, *J. Am. Chem. Soc.*, 1999, **121**, 3968; (c) P. G. Cozzi, *Chem. Soc. Rev.*, 2004, **33**, 410; (d) T. Katsuki, *Chem. Soc. Rev.*, 2004, **33**, 437; (e) A. C. W. Leung and M. J. MacLachlan, *J. Inorg. Organomet. Polym. Mater.*, 2007, 57.
- 11 (a) D. P. Kessissoglou, M. L. Kirk, M. S. Lah, X. Li, C. Raptopoulou, W. E. Hatfield and V. L. Pecoraro, *Inorg. Chem.*, 1992, **31**, 5424; (b) M. Dey, C. P. Rao, P. K. Saarenketo and K. Rissanen, *Inorg. Chem. Commun.*, 2002, **5**, 380; (c) Y. M. Chumakov, V. I. Tsapkov, Yu. A. Simonov, B. Ya. Antosyak, G. Bocelli, M. Perin, Z. A. Starikova, N. M. Samus and A. P. Gulya, *Koord. Khim. (Russ.)*, 2005, **31**, 621.
- 12 I. J. Hewitt, J.-K. Tang, N. T. Madhu, R. Clérac, G. Buth, C. E. Anson and A. K. Powell, *Chem. Commun.*, 2006, **25**, 2650.
- 13 (a) R. H. Blessing, *Acta Cryst.*, 1995, **A51**, 33; (b) CrysAlisPro v171.32, Oxford Diffraction: Wroclaw, Poland, 2008.
- 14 *SHELXTL 6.10*, Bruker Analytical Instrumentation, Madison, Wisconsin, USA, 2000.
- 15 H. Muhonen, W. E. Hatfield and J. H. Helms, *Inorg. Chem.*, 1986, **25**, 800.

- 16 R. S. Downing and F. L. Urbach, *J. Am. Chem. Soc.*, 1969, **91**, 5977.
- 17 P. E. Kruger, G. D. Fallon, B. Moubaraki, K. J. Berry and K. S. Murray, *Inorg. Chem.*, 1995, **34**, 4808.
- 18 (a) J. J. Borrás-Almenar, J. M. Clemente-Juan, E. Coronado and B. Tsukerblat, *Inorg. Chem.* 1999, **38**, 6081; (b) J. J. Borrás-Almenar, J. M. Clemente-Juan, E. Coronado and B. Tsukerblat, *J. Comput. Chem.*, 2001, **22**, 985.
- 19 J. Tercero, E. Ruiz, S. Alvarez, A. Rodríguez-Forteza and P. Alemany, *J. Mater. Chem.*, 2006, **16**, 2729.
- 20 R. egner, M. Gottschaldt, H. Görls, E.-G. Jäger and D. Klemm, *Chem. Eur. J.*, 2001, **7**, 2143
- 21 O. Kahn, *Molecular Magnetism*; VCH Publishers: Weinheim, Germany, 1993
- 22 (a) S. S. Tandon, L. K. Thompson, M. E. Manuel and J. N. Bridson, *Inorg. Chem.*, 1994, **33**, 5555; (b) E. Ruiz, J. Cano, S. Alvarez and P. Alemany, *J. Am. Chem. Soc.*, 1998, **120**, 11122.

Captions for figures

Scheme 1 Two enantiomeric Schiff base ligands, *R*-H₂L and *S*-H₂L.

Scheme 2 (a) Scheme of the magnetic interactions in **1R** according to spin Hamiltonian (eq. 1). (azide is showed instead of 75% azide and 25% bromide ions disorder). (b) Scheme of the magnetic interactions among copper centers in **2R**.

Figure 1 ORTEP drawings of the two similar NaMn₄ clusters (a) and the NaMn^{II}Mn^{III}₃ cores (b) in the asymmetric unit of **1R** (left) and **1S** (right) with thermal ellipsoids at 50% probability (Br ions are showed instead of 75% azide and 25% bromide ions disorder between two Mn^{III} ions as a bridge in the clusters of Mn1.).

Figure 2 ORTEP drawings of the Cu₆ clusters (a) and the Cu^{II}₆ cores (b) in the asymmetric unit of **2R** (left) and **2S** (right) with ellipsoids at 50% probability. The open lines represent the elongated Cu-O bonds in the cubane unit, while the dashed lines represent the eye-guides of the cubane sketch.

Figure 3 Room-temperature CD spectra of **1R**, **1S** and **2R**, **2S** in KBr pellets.

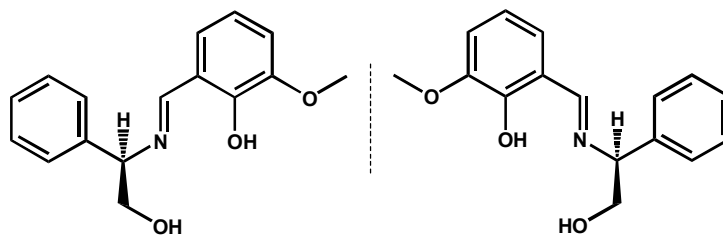
Figure 4 (a) Plots of μ_{eff} as a function of *T* for **1R** and **1S**. (b) Magnetization at 2 K vs. applied field for **1R** and **1S**. (c) Temperature dependence of the effective magnetic moment for **1R** (calculated from magnetization at *B* = 0.05 T), with the low-temperature region expanded in the inset. (d) Field dependence of magnetization for **1R** at *T* = 2 K. Empty circles – experimental data, full lines – calculated data with the spin Hamiltonian and parameters in the text.

Figure 5 (a) Plots of μ_{eff} as a function of *T* for **2R** and **2S**. (b) Magnetization at 2 K vs. applied field for **2R** and **2S**. (c) Temperature dependence of the effective magnetic moment for **2R** (calculated from magnetization at *B* = 0.05 T). Empty circles – experimental data, full lines – calculated data with the spin Hamiltonian and parameters in the text.

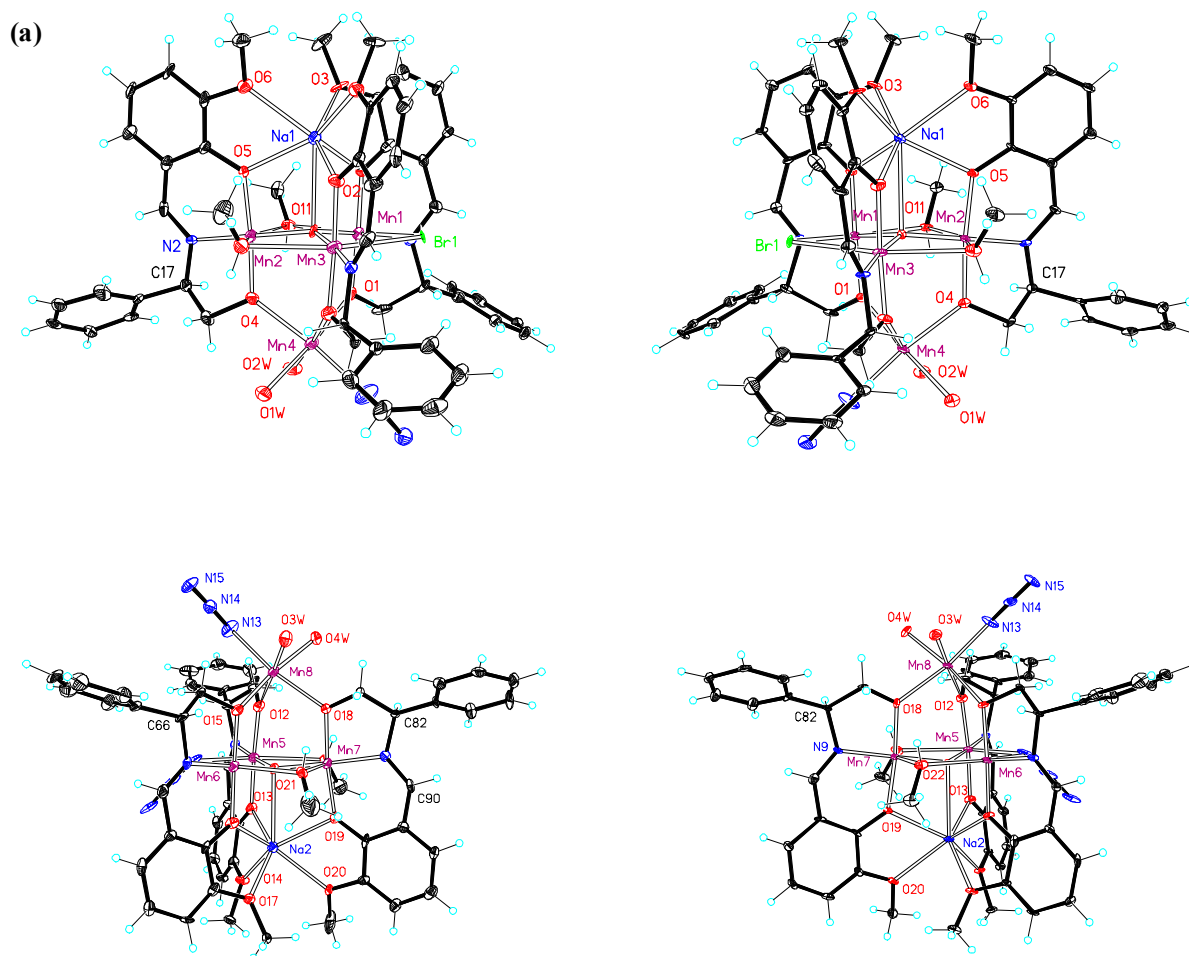
Table 1. Crystal data and structure refinements for **1R**, **1S**, **2R** and **2S**.

compound	1R (150 K)	1S (150 K)	2R (150 K)	2S (150 K)
formula	C ₁₀₂ H ₁₂₂ Br _{4.25} Mn ₈ N _{17.25} Na ₂ O ₃₀	C ₁₀₂ H ₁₂₂ Br _{4.25} Mn ₈ N _{17.25} Na ₂ O ₃₀	C ₆₇ H ₇₆ Cu ₆ N ₂₀ O ₁₉	C ₆₇ H ₇₆ Cu ₆ N ₂₀ O ₁₉
fw	2894.79	2894.79	1846.72	1846.72
cryst syst	monoclinic	monoclinic	orthorhombic	orthorhombic
Space group	<i>P</i> 2 ₁ (No. 4)	<i>P</i> 2 ₁ (No. 4)	<i>P</i> 2 ₁ 2 ₁ 2 ₁ (No. 19)	<i>P</i> 2 ₁ 2 ₁ 2 ₁ (No. 19)
<i>a</i> (Å)	14.0819(3)	13.9942(1)	16.532(12)	16.5932(8)
<i>b</i> (Å)	15.1580(3)	15.1871(1)	20.872(15)	20.8546(15)
<i>c</i> (Å)	26.9984(5)	27.0453(2)	22.005(16)	22.274(3)
α (deg)	90	90	90	90
β (deg)	90.822(2)	90.821(1)	90	90
γ (deg)	90	90	90	90
<i>V</i> (Å ³)	5762.3(2)	5747.38(7)	7593(9)	7707.8(12)
<i>Z</i>	2	2	4	4
<i>D</i> _c (g cm ⁻³)	1.668	1.673	1.616	1.591
μ (mm ⁻¹)	9.392	9.416	1.734	2.498
reflns collected	19383	21957	35350	12932
unique reflns (<i>R</i> _{int})	12483 (0.0396)	11759 (0.0388)	16525 (0.1475)	8799 (0.0353)
params	1468	1468	1025	1025
<i>S</i> on <i>F</i> ²	1.016	0.996	0.958	0.995
<i>R</i> ₁ ^{<i>a</i>} , <i>wR</i> ₂ ^{<i>b</i>} (<i>I</i> > 2σ(<i>I</i>))	0.0770, 0.2163	0.0661, 0.1874	0.0794, 0.1859	0.0406, 0.1016
<i>R</i> ₁ ^{<i>a</i>} , <i>wR</i> ₂ ^{<i>b</i>} (all data)	0.0998, 0.2330	0.0769, 0.1959	0.1139, 0.2148	0.0468, 0.1041
Flack parameter	0.030(9)	0.014(7)	-0.001(19)	-0.02(3)

^{*a*} $R_1 = \sum ||F_o| - |F_c|| / \sum |F_o|$, ^{*b*} $wR_2 = [\sum w(F_o^2 - F_c^2)^2 / \sum w(F_o^2)^2]^{1/2}$



Scheme 1. Two enantiomeric Schiff base ligands: *R*-H₂L and *S*-H₂L.



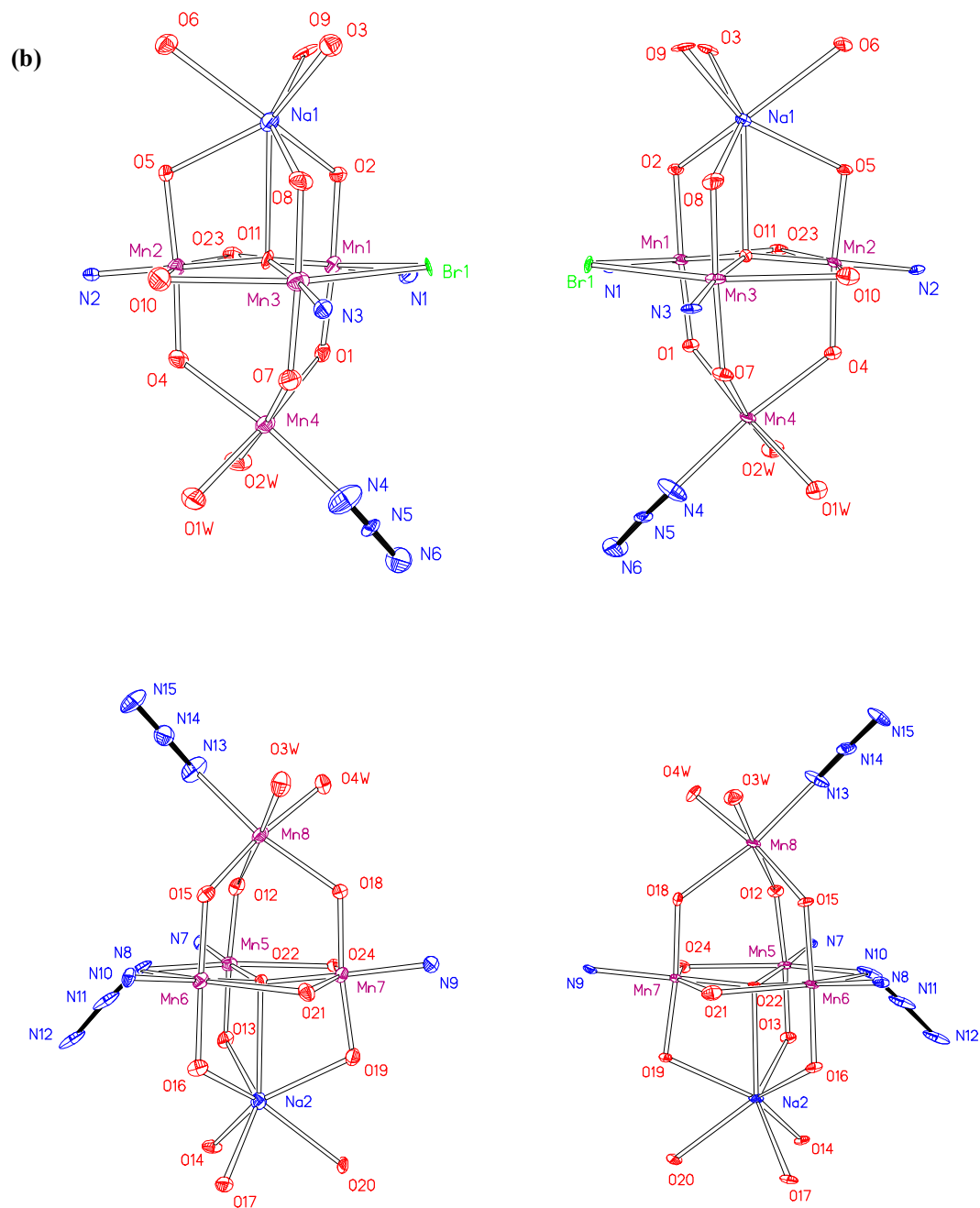


Figure 1. ORTEP drawings of the two similar NaMn_4 clusters (a) and the $\text{NaMn}^{\text{II}}\text{Mn}^{\text{III}}_3$ cores (b) in the asymmetric unit of **1R** (left) and **1S** (right) with ellipsoids at 50% probability (Br ions are shown as green spheres instead of 75% azide and 25% bromide ions disorder between two Mn^{III} ions as a bridge in the clusters of Mn1.).

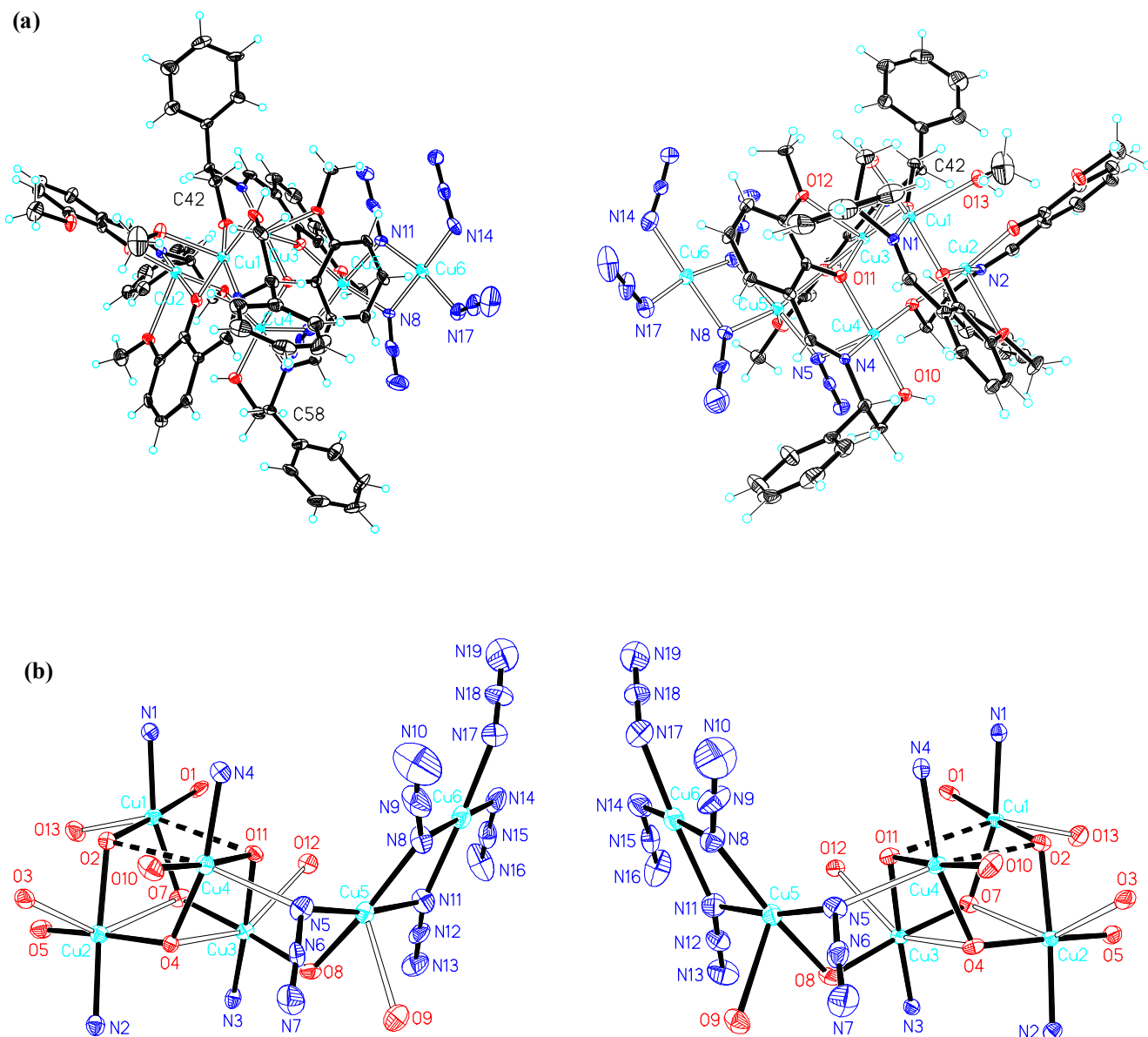


Figure 2. ORTEP drawings of the Cu₆ clusters (a) and the Cu^{II}₆ cores (b) in the asymmetric unit of **2R** (left) and **2S** (right) with ellipsoids at 50% probability. The open lines represent the elongated Cu-O bonds in the cubane unit. The dashed lines represent the weak Cu-O interactions in the cubane unit.

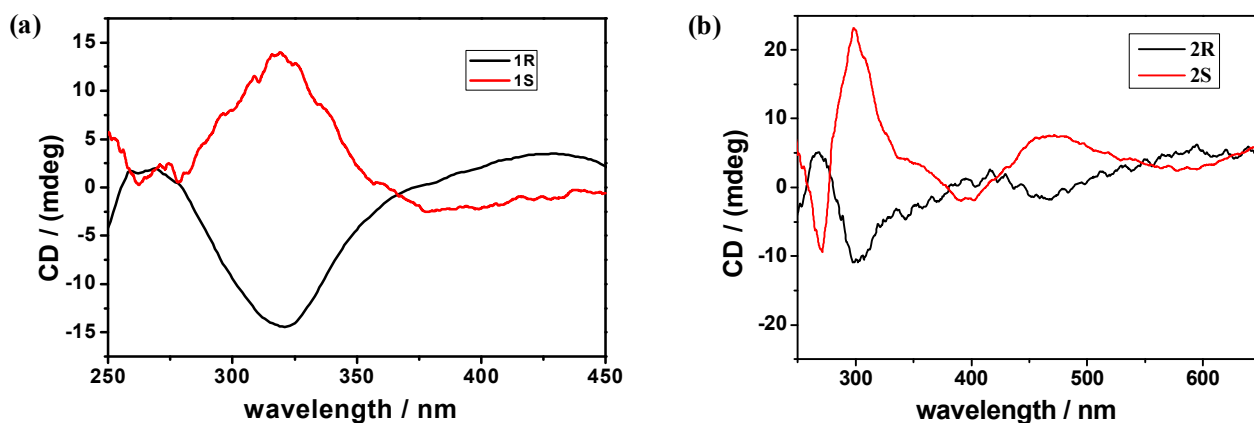


Figure 3 Room-temperature CD spectra of **1R**, **1S** and **2R**, **2S** in KBr pellets.

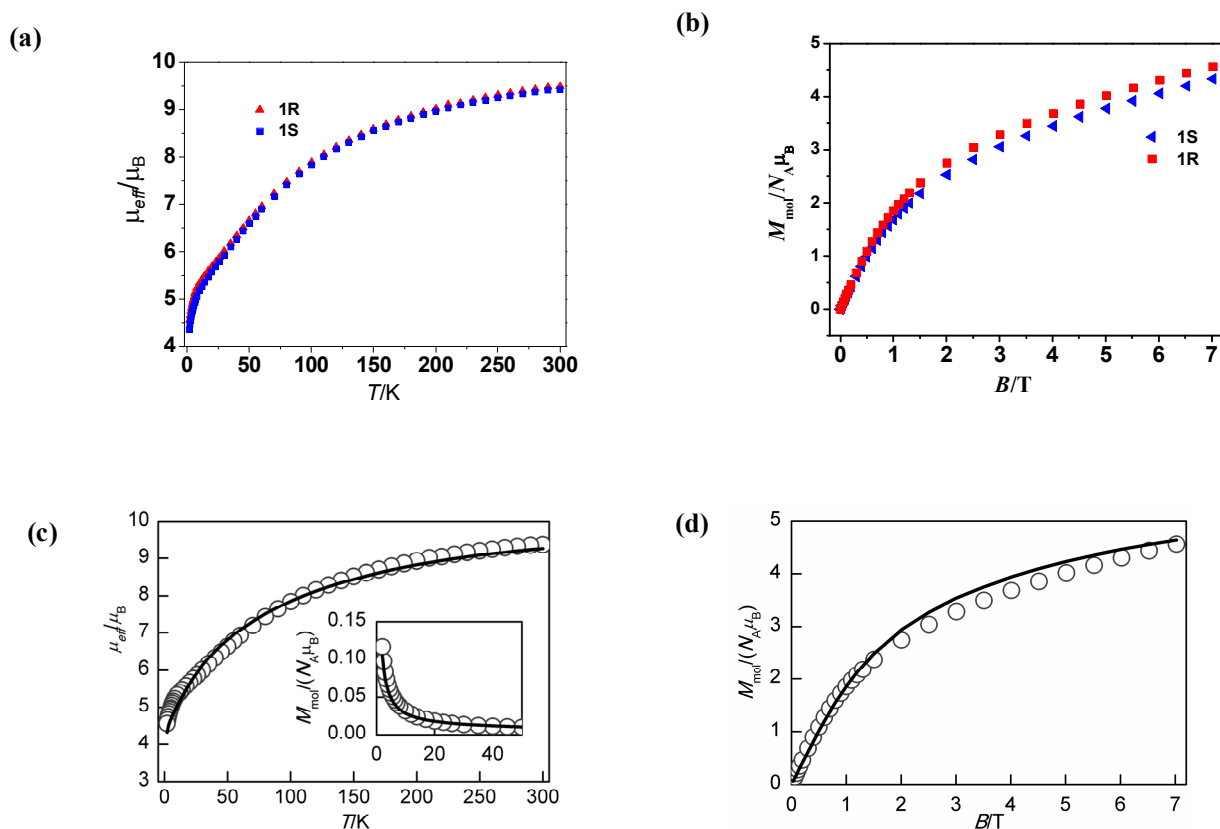
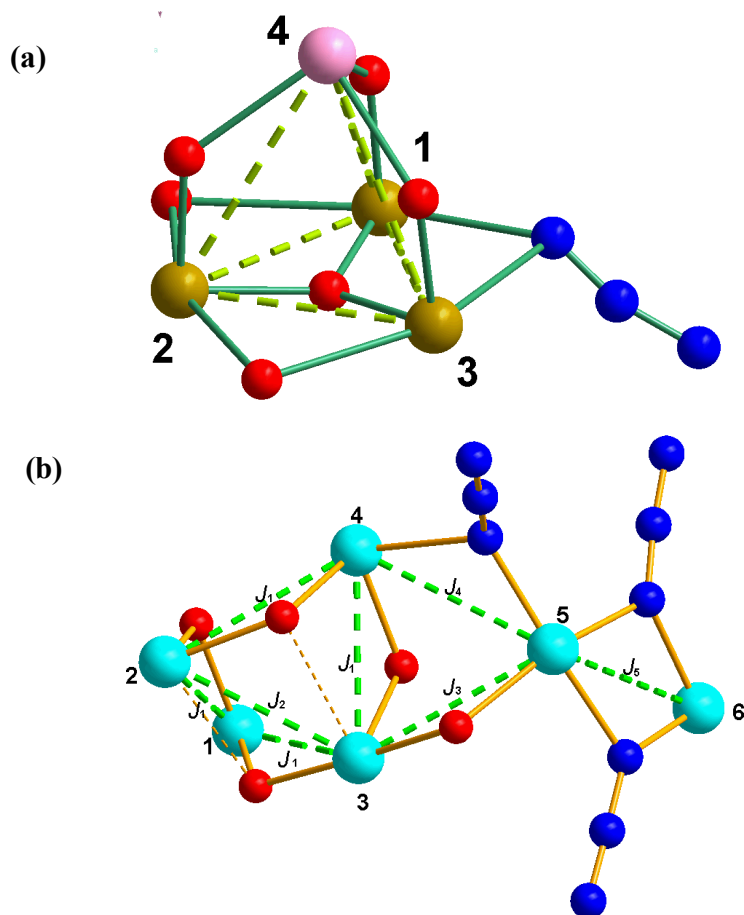
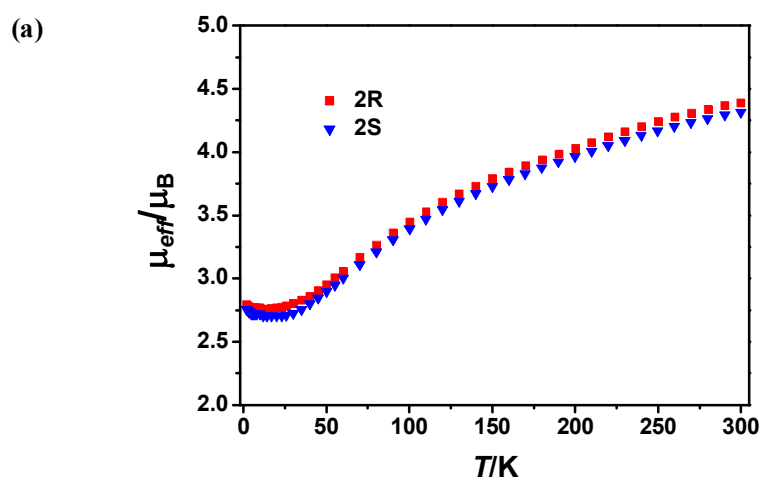


Figure 4 (a) Plots of μ_{eff} a function of T for **1R** and **1S**. (b) Magnetization at 2 K vs. applied field for **1R** and **1S**. (c) Temperature dependence of the effective magnetic moment for **1R** (calculated from magnetization at $B = 0.05$ T), with the low-temperature region expanded in the inset. (d) Field dependence of magnetization for **1R** at $T = 2$ K. Empty circles – experimental data, full lines – calculated data with the spin Hamiltonian and parameters in the text.



Scheme 2 Schemes of the magnetic interactions in **1R** (a) and **2R** (b) (azide is shown to instead of 75% azide and 25% bromide ions disorder).



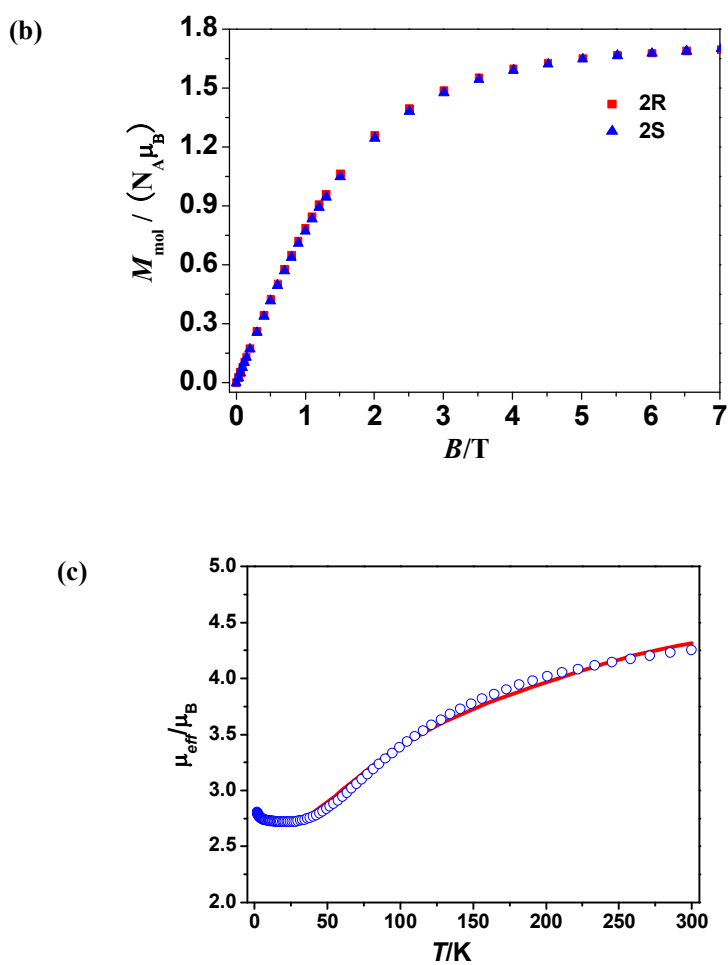


Figure 5 (a) Plots of μ_{eff} a function of T for **2R** and **2S**. (b) Magnetization at 2 K vs. applied field for **2R** and **2S**. (c) Temperature dependence of μ_{eff} for **2R** (triangles – experimental data, full lines – calculated data with the spin Hamiltonian and parameters in the text).

Synopsis for Table of Contents

Two enantiomeric Schiff base ligands *R*-/*S*-H₂L *in situ* generated from *o*-vanillin and *R*- or *S*-2-phenylglycinol were applied to assemble chiral multinuclear magnetic clusters. Two new enantiomorphous Mn^{II}Mn^{III}₃ clusters and two new enantiomorphous Cu^{II}₆ clusters have been synthesized and characterized by X-ray crystallography, CD spectroscopy and magnetism.

